Spin-density-wave instabilities in the organic conductors $(TMTSF)_2ClO_4$: Role of anion ordering

K. Sengupta[1] and N. Dupuis[2]
[1]*Department of Physics, University of Maryland, College Park, Maryland 20742-4111*
[2]*Laboratoire de Physique des Solides, Associé au CNRS, Université Paris-Sud, 91405 Orsay, France*
(Received 13 June 2001; published 19 December 2001)

We study the spin-density-wave (SDW) instabilities in the quasi-one-dimensional conductor $(TMTSF)_2ClO_4$. The orientational order of the anions ClO_4 doubles the unit cell and leads to the presence of two electronic bands at the Fermi level. From the Ginzburg-Landau expansion of the free energy, we determine the low-temperature phase diagram as a function of the strength of the Coulomb potential due to the anions. Upon increasing the anion potential, we first find a SDW phase corresponding to an interband pairing. This SDW phase is rapidly suppressed, the metallic phase being then stable down to zero temperature. The SDW instability is restored when the anion potential becomes of the order of the interchain hopping amplitude. The metal-SDW transition corresponds to an intraband pairing that leaves half of the Fermi surface metallic. At lower temperature, a second transition, corresponding to the other intraband pairing, takes place and opens a gap on the whole Fermi surface. We discuss the consequence of our results for the experimental phase diagram of $(TMTSF)_2ClO_4$ at high magnetic field.

DOI: 10.1103/PhysRevB.65.035108 PACS number(s): 75.30.Fv, 74.70.Kn, 81.30.Dz

I. INTRODUCTION

The organic conductors of the Bechgaard salt family $(TMTSF)_2X$ (where TMTSF stands for tetramethyltetraselenafulvalene and $X=PF_6, ClO_4 \ldots$) exhibit a very rich phase diagram when temperature, magnetic field, or pressure are varied.[1] One of the most remarkable phenomena is the existence of a series of spin-density-wave (SDW) phases in presence of a moderate magnetic field of a few Tesla.[2] These phases are separated by first-order transitions and exhibit a quantization of the Hall effect: $\sigma_{xy}=-2Ne^2/h$ per layer of TMTSF molecules, where the integer N varies at each phase transition.

According to the so-called quantized-nesting model (QNM),[2,3] the formation of the magnetic-field-induced spin-density-wave (FISDW) phases results from an interplay between the nesting properties of the quasi-one-dimensional (Q1D) Fermi surface and the quantization of the electronic orbits in magnetic field. Although the QNM explains the quantization of the Hall effect[4,5] and most features of the phase diagram, deviations from the theoretical predictions have been observed at high magnetic field in the compound $(TMTSF)_2ClO_4$.[6–8] In the last FISDW phase, when the magnetic field exceeds 18 T, the second-order metal-SDW transition that occurs at $T_c \simeq 5.5$ K is followed by a SDW-SDW transition at $T_c' \simeq 3.5$ K. It is believed that the existence of this low-temperature SDW phase is due to the orientational ordering of the (noncentrosymmetric) anions ClO_4 that occurs at $T_{AO} \simeq 24$ K in slowly cooled (relaxed) samples.[1,6] Nevertheless, to our knowledge, there is no satisfying theoretical description[9] of the phase diagram of $(TMTSF)_2ClO_4$ at high field in spite of recent progress.[10–12]

In this paper, we study the effect of anion ordering on the SDW phase in the absence of a magnetic field. In relaxed samples, the ground state of $(TMTSF)_2ClO_4$ is superconducting in the absence of a magnetic field. Therefore, our study of the SDW in presence of anion ordering does not apply directly to the experimental situation. Nevertheless, it is the first step towards the understanding of the behavior of $(TMTSF)_2ClO_4$ at high field. Our work shows that in previous analysis[13–15,10,11] (with or without magnetic field), the anion ordering was not accounted for properly. Because of the anion potential, the SDW order parameter necessarily has two Fourier components. As a result, the metal-SDW transition temperature is determined by a *generalized* Stoner criterion. This point has been systematically overlooked, which, therefore, calls for a revision of previous works.

The results obtained in this paper are based on a simple model, where the anion ordering is assumed to create an electrostatic potential $V(-V)$ on even (odd) chains. Moreover, the crystal structure is taken to be orthorhombic, while the actual structure of the Bechgaard salts is triclinic. In the spirit of the QNM, we expect such a simple model (with a few unknown parameters) to correctly describe the physics of $(TMTSF)_2ClO_4$. The anion potential $\pm V$ doubles the crystal periodicity in the transverse direction. This leads to a reduced Brillouin zone with two electronic bands crossing the Fermi level (Fig. 1) in qualitative agreement with the actual Fermi surface of $(TMTSF)_2ClO_4$ as obtained from quantum chemistry calculation.[16] Instead of a single (best) nesting vector, there are three possible nesting vectors: $\mathbf{Q}_{\rm inter}$ (interband pairing), $\mathbf{Q}_+$, and $\mathbf{Q}_-$ (intraband pairing). The instability that does occur at low temperature depends on the ratio V/t_b between the anion potential and the interchain hopping amplitude t_b. It has recently been shown, both from quantum chemistry calculation[16] and experiments,[17] that V can be of the order of t_b.

In Sec. II, we calculate the electron-hole susceptibility within the random-phase approximation (RPA) and thus obtain the transition temperature between the metallic phase and the SDW phase. The complete phase diagram is obtained from the Ginzburg-Landau expansion of the free energy

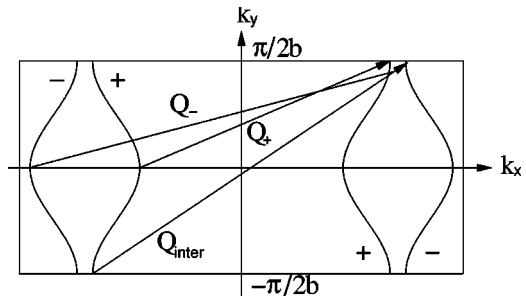

FIG. 1. Possible nesting vectors in presence of the anion potential. $\mathbf{Q}_{\rm inter}(\mathbf{Q}_{\pm})$ corresponds to interband (intraband) pairing. The magnitude of the band splitting at $k_y=\pm\pi/2b$ equals $2V$, where V is the strength of the anion potential (see text).

(Sec. III). For a weak anion potential ($V\ll t_b$), we find that the SDW phase corresponds to the interband pairing ($\mathbf{Q}_{\rm inter}$). The transition temperature is strongly suppressed by the anion potential and in general vanishes above a critical value of V. The SDW instability is restored when V becomes of the order of the interchain hopping amplitude ($V\sim t_b$). The metal-SDW transition corresponds to the intraband pairing $\mathbf{Q}_+$ (or $\mathbf{Q}_-$). Half of the Fermi surface remains gapless, so that the SDW phase is metallic. At lower temperature, a second SDW instability occurs at the (intraband) nesting vector $\mathbf{Q}_-$ (or $\mathbf{Q}_+$), thus opening a gap on the whole Fermi surface.

Some of our conclusions agree with the results of Kishigi and co-workers.[10–12] In particular, these authors have shown that the anion potential may stabilize SDW phases with wave vectors $\mathbf{Q}_{\rm inter}$, $\mathbf{Q}_-$, $\mathbf{Q}_+$ (or $\mathbf{Q}_-$ and $\mathbf{Q}_+$).[18]

II. INSTABILITY OF THE METALLIC PHASE

In Q1D materials, the Fermi surface consists of two slightly warped open sheets. As a result, in the vicinity of the Fermi level, the electron dispersion is well approximated as

$$\epsilon_\alpha(k_x,k_y)=v_F(\alpha k_x-k_F)+t_\perp(k_y b), \tag{2.1}$$

where k_x and k_y are the electron momenta along and across the conducting chains, and b is the interchain spacing. Here and in the rest of the paper, we neglect the third direction (z axis) that does not play an important role for our purpose, and use natural units $\hbar=k_B=c=1$. In Eq. (2.1), the longitudinal electron dispersion is linearized in k_x in the vicinity of the two 1D Fermi points $\pm k_F$, and $v_F=2at_a\sin(k_F a)$ is the corresponding Fermi velocity. t_a is the transfer integral along the chain and a the lattice spacing. $\alpha=-,+$ corresponds to the left and the right Fermi sheets. The transverse dispersion $t_\perp(k_y b)$ is given by

$$t_\perp(k_y b)=t_\perp^{\rm odd}(k_y b)+t_\perp^{\rm even}(k_y b), \tag{2.2}$$

$$t_\perp^{\rm even}(k_y b)=-2t_{2b}\cos(2k_y b), \tag{2.3}$$

$$t_\perp^{\rm odd}(k_y b)=-2t_b\cos(k_y b)-2t_{3b}\cos(3k_y b), \tag{2.4}$$

where t_{nb} is the transfer integral for electron hopping to the nth neighboring chain. $t_\perp^{\rm odd}$ and $t_\perp^{\rm even}$ correspond to odd and even n, respectively. For a simple model with only nearest-neighbor hopping, i.e., when $t_{2b}=t_{3b}=0$, the linearized dispersion (2.1) satisfies the property $\epsilon_-(\mathbf{k})=-\epsilon_+(\mathbf{k}+\mathbf{Q}_0)$, which corresponds to a perfect nesting of the Fermi surface at wave vector $\mathbf{Q}_0=(2k_F,\pi/b)$. For $t_{2b},t_{3b}\neq 0$, the nesting becomes imperfect. Consequently, the nesting vector shifts to $\mathbf{Q}=(2k_F+\delta q_x,\pi/b+\delta q_y)$ and the SDW phase occurs with lower transition temperature. Generally, t_{3b} is neglected since it is very small, i.e., $t_{3b}/t_b\ll 1$. However, as we shall see, t_{3b} plays an important role in the SDW phases with intraband nesting vectors $\mathbf{Q}_+$ and $\mathbf{Q}_-$, and should, therefore, be retained.

The anion potential in Q1D systems can be most simply modeled as $V_{\rm anion}=V(-1)^n$, where n is the chain index. In the presence of the anion potential, the Hamiltonian of the system in the absence of electron-electron interaction can be written as

$$H_0=\int d^2r\sum_{\alpha,\sigma}\hat\psi^\dagger_{\alpha\sigma}(\mathbf{r})[v_F(\alpha\hat k_x-k_F)+t_\perp(\hat k_y b)+V(-1)^n]\hat\psi_{\alpha\sigma}(\mathbf{r}), \tag{2.5}$$

where the $\hat\psi_{\alpha\sigma}$'s are fermionic operators for right ($\alpha=+$) and left ($\alpha=-$) moving particles, and $\sigma=\uparrow,\downarrow$ is the spin index. $\mathbf{r}=(x,nb)$, and $\hat k_x,\hat k_y$ are momentum operators along x and y.

The Hamiltonian (2.5) can be diagonalized to obtain the eigenfunctions and energy eigenvalues,

$$\psi^j_{\alpha,\mathbf{k}}(\mathbf{r})=\frac{1}{\sqrt{A}}\exp[i(\mathbf{k}+\mathbf{K}/2)\cdot\mathbf{r}]\sum_{p=\pm}\gamma^{jp}_{k_y}e^{ip\mathbf{K}\cdot\mathbf{r}/2}, \tag{2.6}$$

$$\epsilon^j_{\alpha,\mathbf{k}}=v_F(\alpha k_x-k_F)+\epsilon^j_{k_y}, \tag{2.7}$$

where $j=\pm$, $A=L_xL_y$ is the area of the system, $\mathbf{K}=(0,\pi/b)$, and $k_y\in[-\pi/2b,\pi/2b]$ reflecting period doubling along y due to the presence of the anion potential. The transverse momentum dependent part of the energy $\epsilon^j_{k_y}$ is given by

$$\epsilon^j_{k_y}=j\sqrt{V^2+[t_\perp^{\rm odd}(k_y b)]^2}+t_\perp^{\rm even}(k_y b). \tag{2.8}$$

The presence of the anion potential splits the energy dispersions into two bands with energies $\epsilon^+_{\alpha,\mathbf{k}}$ and $\epsilon^-_{\alpha,\mathbf{k}}$ as shown in Fig. 1. The factors $\gamma^{jp}_{k_y}$ are given by

$$\gamma^{++}_{k_y}=\gamma^{--}_{k_y}=\frac{1}{\sqrt{2}}\left(1-\frac{t_\perp^{\rm odd}(k_y b)}{\sqrt{[t_\perp^{\rm odd}(k_y b)]^2+V^2}}\right)^{1/2},$$

$$\gamma^{+-}_{k_y}=-\gamma^{-+}_{k_y}=\frac{1}{\sqrt{2}}\left(1+\frac{t_\perp^{\rm odd}(k_y b)}{\sqrt{[t_\perp^{\rm odd}(k_y b)]^2+V^2}}\right)^{1/2}. \tag{2.9}$$

The amplitude of the wave function at $\mathbf{r}=(x,nb)$ depends on the factors $\gamma^{jp}_{k_y}$ and is given by

$$|\psi^{j}_{\alpha,\mathbf{k}}(\mathbf{r})| = |\gamma^{j+}_{k_y} + (-1)^n \gamma^{j-}_{k_y}|. \tag{2.10}$$

Electronic states in the $+(-)$ band have a higher probability amplitude on even (odd) chains. This localization becomes very important when $V \gtrsim \sqrt{2} t_b$ (assuming $t_{3b} \ll t_b$, which is obviously the case for a realistic dispersion law). In this regime, even and odd chains tend to decouple, and the dispersion law reduces to $\epsilon^{j}_{\alpha,\mathbf{k}} \simeq v_F(\alpha k_x - k_F) + jV + t_\perp^{\text{even}}(k_y b)$.

Using Eqs. (2.6) and (2.7), we obtain the Green functions in the absence of electron-electron interaction,

$$G_{\alpha\sigma}(\mathbf{r},\mathbf{r}';\omega_n) = \sum_{j,\mathbf{k}} \frac{\psi^{j}_{\alpha,\mathbf{k}}(\mathbf{r})\,\psi^{j\,*}_{\alpha,\mathbf{k}}(\mathbf{r}')}{i\omega_n - \epsilon^{j}_{\alpha,\mathbf{k}}}, \tag{2.11}$$

where ω_n is a fermionic Matsubara frequency.

A. Bare susceptibilities

Due to the presence of two electronic bands, there are three possible SDW instabilities with wave vectors $\mathbf{Q}_+$, $\mathbf{Q}_-$, and $\mathbf{Q}_{\text{inter}}$ as shown in Fig. 1. $\mathbf{Q}_+$ and $\mathbf{Q}_-$ are intraband nesting vectors that satisfy $(Q_y)_\pm \approx \pi/2b$. $\mathbf{Q}_{\text{inter}}$ is the interband nesting vector [with $(Q_y)_{\text{inter}} \approx \pi/b$]. In the absence of the anion potential, the SDW instability occurs with $\mathbf{Q} = \mathbf{Q}_{\text{inter}}$. To obtain a quantitative description of these possible instabilities and the phase diagram for the system, we calculate the susceptibility $\chi(\mathbf{q},\mathbf{q}')$ in the particle-hole channel within the RPA. First, let us consider the susceptibilities in the absence of electron-electron interaction,

$$\chi^0_{\alpha\sigma}(\mathbf{r},\mathbf{r}';\tau-\tau') = \langle \mathcal{T}_\tau \hat{\Delta}_{\alpha\sigma}(\mathbf{r},\tau)\hat{\Delta}^\dagger_{\alpha\sigma}(\mathbf{r}',\tau')\rangle_0, \tag{2.12}$$

where $\hat{\Delta}_{\alpha\sigma}(\mathbf{r},\tau) = \hat{\psi}^\dagger_{\overline{\alpha}\sigma}(\mathbf{r},\tau)\hat{\psi}_{\alpha\sigma}(\mathbf{r},\tau)$, τ is an imaginary time, and $\mathcal{T}_\tau$ is the time-ordering operator. The mean value in Eq. (2.12) has to be taken with the Hamiltonian H_0. We use the notation $\overline{\alpha} = -\alpha$, and $\overline{\sigma} = \downarrow,\uparrow$ for $\sigma = \uparrow,\downarrow$. In frequency domain, χ^0 can be expressed in terms of the Green function (2.11) as

$$\chi^0_{\alpha\sigma}(\mathbf{r},\mathbf{r}';p_n) = -T\sum_{\omega_n} G_{\alpha\sigma}(\mathbf{r},\mathbf{r}';\omega_n) G_{\overline{\alpha\sigma}}(\mathbf{r}',\mathbf{r};\omega_n - p_n), \tag{2.13}$$

where p_n is a bosonic Matsubara frequency. For studying the instabilities of the metallic phase, it is sufficient to compute the static susceptibilities $\chi^0_{\alpha\sigma}(\mathbf{r},\mathbf{r}';p_n=0) \equiv \chi^0_{\alpha\sigma}(\mathbf{r},\mathbf{r}')$. Using Eqs. (2.6), (2.7), (2.9), and (2.11), we find

$$\begin{aligned}\chi^0_{\alpha\sigma}(\mathbf{q},\mathbf{q}) = \frac{1}{A}\sum_{\mathbf{k}} \{&[\overline{\chi}^{++}_{\alpha\sigma}(\mathbf{k},\mathbf{q}) + \overline{\chi}^{--}_{\alpha\sigma}(\mathbf{k},\mathbf{q})] \\ &\times (\gamma^{++}_{k_y}\gamma^{++}_{k_y-q_y} + \gamma^{+-}_{k_y}\gamma^{+-}_{k_y-q_y})^2 \\ &+ [\overline{\chi}^{+-}_{\alpha\sigma}(\mathbf{k},\mathbf{q}) + \overline{\chi}^{-+}_{\alpha\sigma}(\mathbf{k},\mathbf{q})] \\ &\times (\gamma^{++}_{k_y}\gamma^{+-}_{k_y-q_y} - \gamma^{++}_{k_y-q_y}\gamma^{+-}_{k_y})^2\},\end{aligned} \tag{2.14}$$

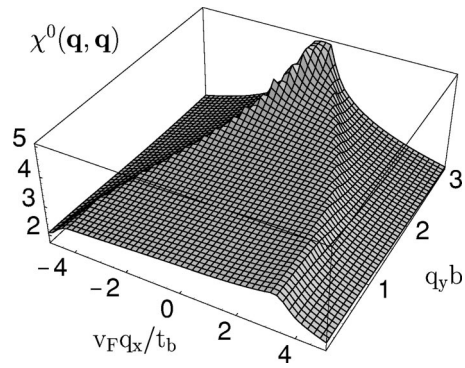

FIG. 2. Susceptibility $\chi^0(\mathbf{q},\mathbf{q})$ in the absence of anion ordering ($V=0$). Here $\chi^0 \equiv \chi^0_{+\uparrow} = \chi^0_{+\downarrow}$, and q_x is measured from $2k_F$. The maximum is located at the interband nesting vector $\mathbf{Q}_{\text{inter}}$ with $(Q_{\text{inter}})_y \approx \pi/b$. The susceptibilities shown in Figs. 2–4 are obtained for $T = 0.02t_b$, $t_{2b} = 0.1t_b$ and $t_{3b} = 0.02t_b$.

$$\begin{aligned}\chi^0_{\alpha\sigma}(\mathbf{q},\mathbf{q}+\mathbf{K}) = \frac{1}{A}\sum_{\mathbf{k}} \{&[\overline{\chi}^{++}_{\alpha\sigma}(\mathbf{k},\mathbf{q}) - \overline{\chi}^{--}_{\alpha\sigma}(\mathbf{k},\mathbf{q})] \\ &\times (\gamma^{++}_{k_y}\gamma^{++}_{k_y-q_y} + \gamma^{+-}_{k_y}\gamma^{+-}_{k_y-q_y}) \\ &+ [\overline{\chi}^{+-}_{\alpha\sigma}(\mathbf{k},\mathbf{q}) - \overline{\chi}^{-+}_{\alpha\sigma}(\mathbf{k},\mathbf{q})] \\ &\times (\gamma^{++}_{k_y}\gamma^{+-}_{k_y-q_y} - \gamma^{++}_{k_y-q_y}\gamma^{+-}_{k_y})\},\end{aligned} \tag{2.15}$$

where

$$\overline{\chi}^{jj'}_{\alpha\sigma}(\mathbf{k},\mathbf{q}) = -T\sum_{\omega_n} (i\omega_n - \epsilon^{j}_{\alpha,\mathbf{k}})^{-1}(i\omega_n - \epsilon^{j'}_{\alpha,\mathbf{k}-\mathbf{q}})^{-1}. \tag{2.16}$$

Notice that due to the presence of the anion potential, the static susceptibilities have a nonzero off-diagonal component $\chi^0(\mathbf{q},\mathbf{q}+\mathbf{K})$. The sum over k_x in Eqs. (2.14) and (2.15) can be analytically calculated using

$$\begin{aligned}&\frac{1}{bL_x}\sum_{k_x} \overline{\chi}^{jj'}_{\alpha\sigma}(\mathbf{k},\mathbf{q}) \\ &= \frac{N(0)}{2}\left\{\ln\left(\frac{2\gamma E_0}{\pi T}\right) + \Psi\left(\frac{1}{2}\right)\right. \\ &\quad \left. - \mathrm{Re}\,\Psi\left[\frac{1}{2} - \frac{v_F(\alpha q_x - 2k_F) + \epsilon^{j}_{k_y} + \epsilon^{j'}_{k_y-q_y}}{4\pi i T}\right]\right\},\end{aligned} \tag{2.17}$$

but the k_y sum needs to be evaluated numerically. In Eq. (2.17), $N(0) = 1/\pi v_F b$ is the density of states per spin at Fermi energy, $E_0 \sim t_a$ an ultraviolet cutoff energy, $\gamma \simeq 1.783$ the exponential of the Euler constant, Ψ the digamma function, and $\mathrm{Re}\,\Psi$ means real part of Ψ. Note that when $V = 0, \chi^0_{\alpha\sigma}(\mathbf{q},\ \mathbf{q}+\mathbf{Q}) = 0$ and the susceptibility becomes diagonal in momentum space.

To find the effect of the anion potential V on the bare susceptibilities, we plot $\chi^0(\mathbf{q},\mathbf{q})$ and $\chi^0(\mathbf{q},\mathbf{q}+\mathbf{K})$ for different values of V/t_b in Figs. 2–4. Here $\chi^0 \equiv \chi^0_{+\uparrow} = \chi^0_{+\downarrow}$, and $\mathbf{q}$

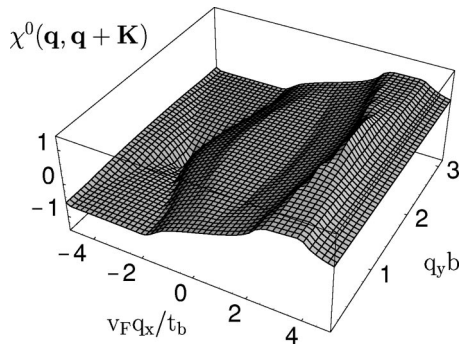

FIG. 3. Off-diagonal component $\chi^0(\mathbf{q},\mathbf{q}+\mathbf{K})$ of the susceptibility for $V/t_b=1$. The notations are the same as in Fig. 2.

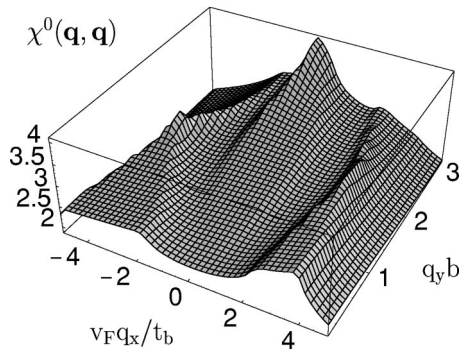

FIG. 4. Diagonal component $\chi^0(\mathbf{q},\mathbf{q})$ of the susceptibility for $V/t_b=1$. Besides the maximum at $\mathbf{Q}_{\rm inter}$, there are two peaks at $q_y=\pi/2b$ corresponding to the intraband nesting vectors $\mathbf{Q}_+$ and $\mathbf{Q}_-$. The notations are the same as in Fig. 2.

is chosen such that $q_x\sim 2k_F$. For $V/t_b=0$, χ^0 is diagonal in momentum space and the peak of $\chi^0(\mathbf{q},\mathbf{q})$ is located at $\mathbf{Q}_{\rm inter}$ with $(Q_{\rm inter})_y\approx\pi/b$ (Fig. 2). The position of the peak moves away from π/b when deviations from perfect nesting due to t_{2b} and t_{3b} become important. As we increase V/t_b, $\chi^0(\mathbf{q},\mathbf{q}+\mathbf{K})$ becomes nonzero and develops peaks at $q_y\approx\pm\pi/2b$ as shown, for $V/t_b=1$, in Fig. 3. The maximum of $\chi^0(\mathbf{q},\mathbf{q})$ [i.e., $\chi^0(\mathbf{Q}_{\rm inter},\mathbf{Q}_{\rm inter})$] reduces in height and two additional peaks develop at $\mathbf{Q}_+$ and $\mathbf{Q}_-$ [with $(Q_\pm)_y=\pi/2b$]. The development of these additional peaks in $\chi^0(\mathbf{q},\mathbf{q})$ can be seen by comparing Figs. 2 and 4. When V is strong enough, the maximum of χ^0 moves from $\mathbf{Q}_{\rm inter}$ to $\mathbf{Q}_+$ or $\mathbf{Q}_-$. We, therefore, expect the SDW wave vector to shift from $\mathbf{Q}_{\rm inter}$ to $\mathbf{Q}_+$ and/or $\mathbf{Q}_-$ as V exceeds a critical value (assuming that the anion potential V does not suppress the SDW instability). Our results for the diagonal susceptibility $\chi^0(\mathbf{q},\mathbf{q})$ are similar to those of Ref. 12.

B. RPA calculation

To find the critical value of the anion potential and to obtain the phase diagram, we now compute the susceptibilities for the interacting system within RPA. We model the interaction using the g-ology model keeping only g_2 to be nonzero,[19]

$$H_{\rm int}=\frac{g_2}{2}\sum_{\alpha,\sigma,\sigma'}\int d^2r\,\hat\psi^\dagger_{\alpha\sigma}(\mathbf{r})\hat\psi^\dagger_{\bar\alpha\sigma'}(\mathbf{r})\hat\psi_{\bar\alpha\sigma'}(\mathbf{r})\hat\psi_{\alpha\sigma}(\mathbf{r}). \tag{2.18}$$

Using the interaction Hamiltonian given by Eq. (2.18), we obtain the susceptibilities by summing the RPA diagrams shown in Fig. 5,

$$\chi_{\alpha\sigma}(\mathbf{q},\mathbf{q}')=\chi^0_{\alpha\sigma}(\mathbf{q},\mathbf{q}')+g_2\sum_{\mathbf{q}''}\chi^0_{\alpha\sigma}(\mathbf{q},\mathbf{q}'')\chi_{\alpha\sigma}(\mathbf{q}'',\mathbf{q}'). \tag{2.19}$$

Substituting Eqs. (2.14) and (2.15) in Eq. (2.19), we find that $\chi_{\alpha\sigma}(\mathbf{q},\mathbf{q}')$ is nonzero only when $\mathbf{q}'=\mathbf{q}$ or $\mathbf{q}+\mathbf{K}$ and is given by

$$\chi_{\alpha\sigma}(\mathbf{q},\mathbf{q})=\{\chi^0_{\alpha\sigma}(\mathbf{q},\mathbf{q})[1-g_2\chi^0_{\alpha\sigma}(\mathbf{q}+\mathbf{K},\mathbf{q}+\mathbf{K})]+g_2[\chi^0_{\alpha\sigma}(\mathbf{q},\mathbf{q}+\mathbf{K})]^2\}/D, \tag{2.20}$$

$$\chi_{\alpha\sigma}(\mathbf{q},\mathbf{q}+\mathbf{K})=\chi^0_{\alpha\sigma}(\mathbf{q},\mathbf{q}+\mathbf{K})/D, \tag{2.21}$$

$$D=[1-g_2\chi^0_{\alpha\sigma}(\mathbf{q},\mathbf{q})][1-g_2\chi^0_{\alpha\sigma}(\mathbf{q}+\mathbf{K},\mathbf{q}+\mathbf{K})]-g_2^2[\chi^0_{\alpha\sigma}(\mathbf{q},\mathbf{q}+\mathbf{K})]^2. \tag{2.22}$$

A SDW instability occurs when the susceptibilities $\chi^0_{\alpha\sigma}(\mathbf{q},\mathbf{q})$ and $\chi^0_{\alpha\sigma}(\mathbf{q},\mathbf{q}+\mathbf{K})$ diverge, i.e., when the denominator D in Eqs. (2.20) and (2.21) vanishes. This yields a generalized Stoner criterion for a SDW instability at wave vector $\mathbf{Q}$,

$$[1-g_2\chi^0(\mathbf{Q},\mathbf{Q})][1-g_2\chi^0(\mathbf{Q}+\mathbf{K},\mathbf{Q}+\mathbf{K})]-g_2^2[\chi^0(\mathbf{Q},\mathbf{Q}+\mathbf{K})]^2=0, \tag{2.23}$$

where $\mathbf{Q}$ is chosen such that $Q_x\sim 2k_F$. This equation is the same for $\mathbf{Q}$ and $\mathbf{Q}+\mathbf{K}$ (reflecting the fact that the SDW contains Fourier components at $\mathbf{Q}$ and $\mathbf{Q}+\mathbf{K}$). We choose to label the SDW phase by the wave vector $\mathbf{Q}$ such that $\chi^0(\mathbf{Q},\mathbf{Q})>\chi^0(\mathbf{Q}+\mathbf{K},\mathbf{Q}+\mathbf{K})$. Note that the off-diagonal component of the susceptibility, i.e., $\chi^0(\mathbf{Q},\mathbf{Q}+\mathbf{K})$, has been systematically overlooked in previous works on the effect of anion ordering in $(TMTSF)_2ClO_4$. As a result, the simple (but wrong) criterion $1-g_2\chi^0(\mathbf{Q},\mathbf{Q})=0$ has been used to determine the SDW transition temperature instead of the generalized Stoner criterion given in Eq. (2.23).

Eq. (2.23) has to be numerically solved to obtain the transition temperature $T_c(V)$ as a function of the anion potential V. The qualitative nature of the phase diagram, however, can be understood qualitatively from Eq. (2.23) without numerical computation. For $V=0$, the off-diagonal susceptibility $\chi^0(\mathbf{Q},\mathbf{Q}+\mathbf{K})=0$ and Eq. (2.23) reduces to $1-g_2\chi^0(\mathbf{Q},\mathbf{Q})=0$. The SDW instability occurs with the nesting wave vector $\mathbf{Q}_{\rm inter}$ corresponding to the maximum of the bare susceptibility χ^0. When V increases, the wave functions become more and more localized on even or odd chains. Since $\mathbf{Q}_{\rm inter}$ corresponds to pairing of electron and hole on chains of op-

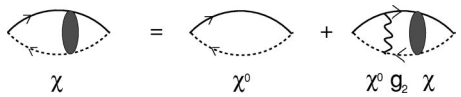

FIG. 5. Feynman diagrams for χ within RPA.

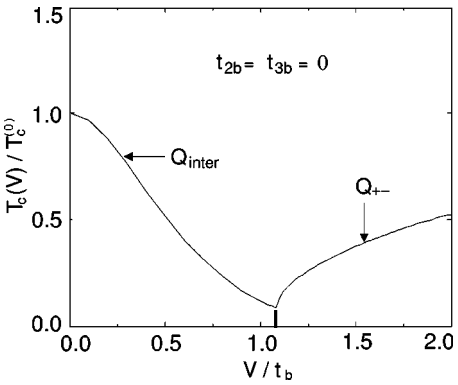

FIG. 6. Phase diagram with $t_{2b}=t_{3b}=0$. The thick vertical line is a guide to the eye for estimating the critical potential at which the transition from $\mathbf{Q}_{\text{inter}}$ to $\mathbf{Q}_{\pm}$ takes place. For $V>V_c\simeq 1.1t_b$, there is coexistence of two SDW's (with wave vectors $\mathbf{Q}_+$ and $\mathbf{Q}_-$) below the transition line (see Sec. III C).

posite parity, T_c drops, until at some critical value of the anion potential, V_{c1}, there is no SDW instability with $\mathbf{Q}=\mathbf{Q}_{\text{inter}}$. [Note that the anion potential does not affect the nesting at $\mathbf{Q}_{\text{inter}}$, which is limited by t_{2b} in our model.] Simultaneously, the pairing with $\mathbf{Q}=\mathbf{Q}_+$ and/or $\mathbf{Q}_-$ becomes increasingly favorable, due to both the wave-function localization and an improved nesting, and eventually at a value of the anion potential, $V_{c2}\sim t_b$, the SDW phase with $\mathbf{Q}=\mathbf{Q}_+$ and/or $\mathbf{Q}_-$ wins over the metallic phase. Indeed, when $V\gg t_b$, the even and the odd chains tend to decouple. The dispersion law of the two electronic bands ($+$ and $-$) becomes $\epsilon^j_{\alpha,\mathbf{k}}\simeq v_F(\alpha k_x-k_F)+jV+t_\perp^{\text{even}}(k_y b)$, and $T_c(V)\to T_c^{(0)}=(2\gamma E_0/\pi)\exp[-2/N(0)g_2]$, where $T_c^{(0)}$ is the transition temperature for a system with perfect nesting. Higher-order harmonics in the transverse dispersion law, such as t_{4b} (not considered in this paper), would introduce deviations from perfect nesting that survive when $V\to\infty$. They are, however, expected to be very small and can be safely discarded. If $V_{c2}>V_{c1}$, there will be a metallic region in the phase diagram with no SDW instability for $V_{c1}<V<V_{c2}$; otherwise, there will be a transition from the SDW phase with $\mathbf{Q}=\mathbf{Q}_{\text{inter}}$ to the SDW phase with $\mathbf{Q}=\mathbf{Q}_+$ and/or $\mathbf{Q}_-$.

Our numerical calculations show that both the scenarios are possible. The phase diagram with $t_{2b}=t_{3b}=0$ is shown in Fig. 6. In this case, there is a transition between SDW phases with $\mathbf{Q}=\mathbf{Q}_{\text{inter}}$ and $\mathbf{Q}=\mathbf{Q}_{\pm}$ without any intermediate metallic phase. Moreover, the SDW's with $\mathbf{Q}=\mathbf{Q}_{\pm}$ have the same transition temperature. The transition between the SDW phases with $\mathbf{Q}_{\text{inter}}$ and $\mathbf{Q}_{\pm}$ occurs at $V=V_c\approx 1.1t_b$, as indicated by the thick vertical line in Fig. 6.

The phase diagram with more realistic parameters, shown in Fig. 7, is quite different. With $t_{2b}=0.1t_b$ and $t_{3b}=0$, the SDW phase with $\mathbf{Q}_{\text{inter}}$ persists up to $V_{c1}\approx 0.4t_b$. For $V>V_{c1}$, we find a metallic phase till $V=V_{c2}\approx t_b$. For $V>V_{c2}$, the SDW phase with $\mathbf{Q}_{\pm}$ is stabilized. When t_{2b} is strong enough, the SDW at $\mathbf{Q}_{\text{inter}}$ is suppressed (i.e., $V_{c1}=0$), but the transition temperature of the intraband SDW's is not affected. In this case, the metallic phase is stable at $T=0$ up to V_{c2} where the SDW with wave vector $\mathbf{Q}_+$ or $\mathbf{Q}_-$ sets in.

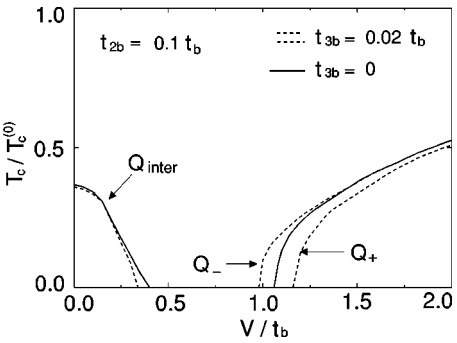

FIG. 7. Phase diagram with nonzero t_{2b} and t_{3b} showing the intermediate metallic region. The solid line indicates the transition temperature when $t_{3b}=0$. Below $T_c^{\text{coex}}\simeq T_c^+$, the two intraband SDW's coexist (see Sec. III C).

The degeneracy between $\mathbf{Q}_+$ and $\mathbf{Q}_-$ is lifted by the presence of a nonszero t_{3b} (Fig. 7). For $t_{3b}>0$, the SDW with wave vector $\mathbf{Q}_-$ has a higher transition temperature, i.e., $T_c^->T_c^+$. The opposite is true when $t_{3b}<0$. It is clear that when $V\gg t_b$, the two SDW's will coexist at low temperature. In this regime, even and odd chains are essentially decoupled, and the two (intraband) instabilities take place almost independently at transition temperatures T_c^+ and T_c^-. This leads to a phase with two coexisting SDW's below $T_c^{\text{coex}}\simeq T_c^+<T_c^-$ (assuming $t_{3b}>0$).

Figure 8 shows the ratio $\delta=[1+\tan(\theta)]/[1-\tan(\theta)]$ of the SDW amplitudes on even and odd chains (see Sec. III D).

III. GINZBURG-LANDAU EXPANSION

In the preceding section, we have shown that two SDW instabilities (at wave vectors $\mathbf{Q}_+$ and $\mathbf{Q}_-$) may occur when V is strong enough. In order to study in more detail the possibility of coexisting SDW's, we derive the Ginzburg-Landau expansion of the free energy and then deduce the phase diagram.

In the presence of two SDW's, the order parameter $\Delta_{\alpha\sigma}(\mathbf{r})=\langle\hat{\Delta}_{\alpha\sigma}(\mathbf{r})\rangle$ takes the general form

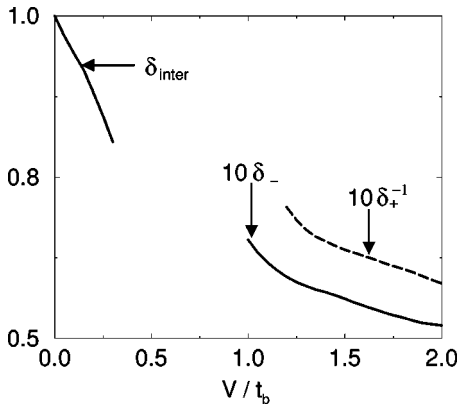

FIG. 8. Ratio $\delta=[1+\tan(\theta)]/[1-\tan(\theta)]$ of the SDW amplitudes on even and odd chains (see Sec. III D). The figure shows δ if $\delta<1$ and δ^{-1} if $\delta>1$. The parameters of the plot are the same as in Fig. 7 (with $t_{3b}=0.02t_b$).

$$\Delta_{\alpha\sigma}(\mathbf{r}) = \sum_{j=\pm,p=\pm} \Delta_{\alpha\sigma}^{jp} \exp\left[i\alpha \left(\mathbf{Q}_j + (p-1)\frac{\mathbf{K}}{2} \right) \cdot \mathbf{r} \right]. \tag{3.1}$$

Note that the SDW with wave vector $\mathbf{Q}_j$ corresponds to a spin modulation with Fourier components $\mathbf{Q}_j$ and $\mathbf{Q}_j+\mathbf{K}$. The order parameter (3.1), which corresponds to electron-hole pairs with opposite spins, assumes the SDW's to be polarized in the (x,y) plane, i.e., $\langle S_z(\mathbf{r})\rangle = 0$. The spin modulation $\langle \mathbf{S}(\mathbf{r})\rangle$ is discussed in more detail below (Sec. III D). The relation $\Delta_{\alpha\sigma}(\mathbf{r}) = \Delta^*_{\alpha\sigma}(\mathbf{r})$ implies that the complex order parameters $\Delta^{jp}_{\alpha\sigma}$ satisfy $\Delta^{jp}_{\alpha\sigma} = \Delta^{jp}_{\alpha\sigma}{}^*$.

Up to quartic order in the order parameter, the free energy (per unit surface) is given by

$$F = g_2 \sum_{\alpha} \int \frac{d^2r}{A} |\Delta_\alpha(\mathbf{r})|^2 + g_2^2 \frac{T}{A} \sum_{\alpha,\omega} \int d^2r_1 d^2r_2 \Delta^*_\alpha(\mathbf{r}_1)\Delta_\alpha(\mathbf{r}_2) G_{\alpha\uparrow}(\mathbf{r}_1,\mathbf{r}_2,\omega) G^-_{\alpha\downarrow}(\mathbf{r}_2,\mathbf{r}_1,\omega) + g_2^4 \frac{T}{2A}$$
$$\times \sum_{\alpha,\omega} \int d^2r_1 d^2r_2 d^2r_3 d^2r_4 \Delta^*_\alpha(\mathbf{r}_1)\Delta_\alpha(\mathbf{r}_2)\Delta^*_\alpha(\mathbf{r}_3)\Delta_\alpha(\mathbf{r}_4) G_{\alpha\uparrow}(\mathbf{r}_1,\mathbf{r}_2,\omega) G^-_{\alpha\downarrow}(\mathbf{r}_2,\mathbf{r}_3,\omega) G_{\alpha\uparrow}(\mathbf{r}_3,\mathbf{r}_4,\omega) G^-_{\alpha\downarrow}(\mathbf{r}_4,\mathbf{r}_1,\omega), \tag{3.2}$$

where $\Delta_\alpha(\mathbf{r}) \equiv \Delta_{\alpha\uparrow}(\mathbf{r})$.

A. Quadratic contribution F_2

Let us first consider the quadratic contribution F_2 to the free energy. One easily obtains

$$F_2 = g_2 \sum_{\alpha,j} (\Delta^{j+}_\alpha{}^*, \Delta^{j-}_\alpha{}^*) \times \begin{pmatrix} 1 - g_2\chi^0(\mathbf{Q}_j,\mathbf{Q}_j) & -g_2\chi^0(\mathbf{Q}_j,\mathbf{Q}_j+\mathbf{K}) \\ -g_2\chi^0(\mathbf{Q}_j+\mathbf{K},\mathbf{Q}_j) & 1 - g_2\chi^0(\mathbf{Q}_j+\mathbf{K},\mathbf{Q}_j+\mathbf{K}) \end{pmatrix} \times \begin{pmatrix} \Delta^{j+}_\alpha \\ \Delta^{j-}_\alpha \end{pmatrix}. \tag{3.3}$$

Introducing the new order parameters $u_{j\alpha}, v_{j\alpha}$ defined by

$$\begin{pmatrix} \Delta^{j+}_\alpha \\ \Delta^{j-}_\alpha \end{pmatrix} = \begin{pmatrix} \cos(\theta_j) & -\sin(\theta_j) \\ \sin(\theta_j) & \cos(\theta_j) \end{pmatrix} \begin{pmatrix} u_{j\alpha} \\ v_{j\alpha} \end{pmatrix}, \tag{3.4}$$

with $\theta_j \in]-\pi/4, \pi/4]$ and

$$\tan(2\theta_j) = \frac{2\chi^0(\mathbf{Q}_j,\mathbf{Q}_j+\mathbf{K})}{\chi^0(\mathbf{Q}_j+\mathbf{K},\mathbf{Q}_j+\mathbf{K}) - \chi^0(\mathbf{Q}_j,\mathbf{Q}_j)}, \tag{3.5}$$

we obtain the diagonal form

$$F_2 = \sum_{\alpha,j} (\lambda^+_j |u_{j\alpha}|^2 + \lambda^-_j |v_{j\alpha}|^2) \tag{3.6}$$

where

$$\lambda^\pm_j = \frac{g_2}{2}[2 - g_2\chi^0(\mathbf{Q}_j,\mathbf{Q}_j) - g_2\chi^0(\mathbf{Q}_j+\mathbf{K},\mathbf{Q}_j+\mathbf{K})] \pm \frac{g_2^2}{2}\mathrm{sgn}[\chi^0(\mathbf{Q}_j+\mathbf{K},\mathbf{Q}_j+\mathbf{K}) - \chi^0(\mathbf{Q}_j,\mathbf{Q}_j)] \times \{[\chi^0(\mathbf{Q}_j,\mathbf{Q}_j) - \chi^0(\mathbf{Q}_j+\mathbf{K},\mathbf{Q}_j+\mathbf{K})]^2 + 4[\chi^0(\mathbf{Q}_j,\mathbf{Q}_j+\mathbf{K})]^2\}^{1/2}. \tag{3.7}$$

The transition temperature T^j_c is determined by

$$\min \lambda^\pm_j(T^j_c) = 0. \tag{3.8}$$

From Eqs. (3.7) and (3.8), one easily recovers the generalized Stoner criterion obtained in the preceding section [Eq. (2.23)]. Since we have assumed $\chi^0(\mathbf{Q}_j,\mathbf{Q}_j) > \chi^0(\mathbf{Q}_j+\mathbf{K},\mathbf{Q}_j+\mathbf{K})$ (see Sec. II B), $\min \lambda^\pm_j = \lambda^+_j$ and the order parameter of the transition is $u_{j\alpha}$. For $T < T^j_c$, we then have $v_{j\alpha} = 0$, i.e.,

$$\Delta^{j-}_\alpha = \tan(\theta_j)\Delta^{j+}_\alpha. \tag{3.9}$$

This equation determines the relative amplitude of the spin modulation on even and odd chains (see Sec. III D). If $T^-_c > T^+_c$ (i.e., $t_{3b} > 0$), then $u_{-\alpha} \neq 0$ when $T < T^-_c$. To determine whether we can have also $u_{+\alpha} \neq 0$ at lower temperature (i.e., coexistence of two SDW's), we must analyze the quartic contribution to the free energy.

B. Quartic contribution F_4

The calculation of the quartic contribution F_4 is somewhat lengthy, and we only give the main results. More details can be found in Appendix A. Using Eqs. (2.6), (2.11), and (3.1), we rewrite the quartic part of the free energy [Eq. (3.2)] as

$$F_4 = \sum_\alpha \sum_{j_1\cdots j_4, p_1\cdots p_4} \delta_{\mathbf{Q}_{j_1}+\mathbf{Q}_{j_3}, \mathbf{Q}_{j_2}+\mathbf{Q}_{j_4}} \times \tilde{B}_\alpha(j_1,j_2,j_3,j_4;p_1,p_2,p_3,p_4) \times \Delta^{j_1p_1}_\alpha{}^* \Delta^{j_2p_2}_\alpha \Delta^{j_3p_3}_\alpha{}^* \Delta^{j_4p_4}_\alpha. \tag{3.10}$$

The coefficients $\tilde{B}_\alpha$ are defined in Appendix A. We now express F_4 as a function of the order parameters $u_{j\alpha}$ and $v_{j\alpha}$. Since the formation of the SDW at wave vector $\mathbf{Q}_j$ corresponds to the order parameter $u_{j\alpha}$, we take $v_{j\alpha} = 0$ in the following. We then obtain a free energy of the form

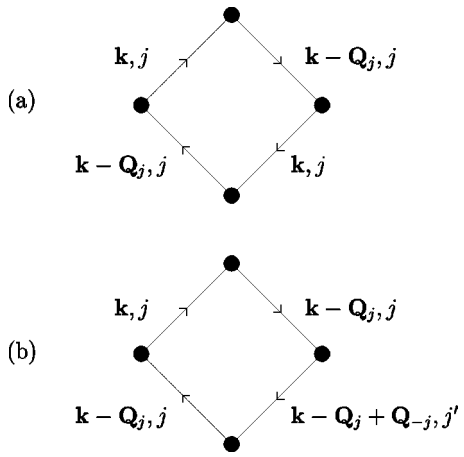

FIG. 9. (a) Main contribution to B_j. (b) A typical diagram contributing to C.

$$F_4=\sum_{\alpha}\left\{\sum_j B_j|u_{j\alpha}|^4+C|u_{+\alpha}u_{-\alpha}|^2\right\}. \tag{3.11}$$

The expression of the coefficients B_j and C is given in Appendix A. The important point here is that the interaction term in Eq. (3.11) is weak, i.e.,

$$\frac{C}{B_j}=O\left(\frac{T^2}{V^2}\right). \tag{3.12}$$

This result is easily obtained by considering the diagrams that contribute to B_j or C. The main contribution to B_j comes from the type of diagrams shown in Fig. 9(a). $\mathbf{Q}_j$ being the best nesting vector for the pairing in the band j, the value of this diagram is essentially determined by the nesting properties. Since the quadratic term F_2 predicts an instability of the metallic phase against the formation of a SDW at wave vector $\mathbf{Q}_j$, the nesting is good (and becomes better with increasing V). Diagrams contributing to C mix the bands $+$ and $-$. A typical diagram is shown in Fig. 9(b). Contrary to diagrams of Fig. 9(a), it is not possible to have all electronic states near the Fermi surface and at least one of them has an energy of order V with respect to the Fermi level. For instance, in the diagram of Fig. 9(b), the state $(\mathbf{k}-\mathbf{Q}_j+\mathbf{Q}_{-j},j')$ has an energy of order V with respect to the Fermi level when the states $(\mathbf{k},j)$ and $(\mathbf{k}-\mathbf{Q}_j,j)$ lie near the Fermi surface. As a result, these diagrams turn out to be of order $(T/V)^2$ with respect to those contributing to B_j (see Appendix A). As shown in the next section, this ensures that at low temperature the two order parameters $u_{+\alpha}$ and $u_{-\alpha}$ coexist.

C. Phase diagram

Collecting the results from the preceding sections, we obtain the following free energy:

$$F=\sum_{\alpha}\left\{\sum_j\left[A_j|u_{j\alpha}|^2+B_j|u_{j\alpha}|^4\right]+C|u_{+\alpha}u_{-\alpha}|^2\right\}, \tag{3.13}$$

where $A_j=\lambda_j^+$.

The free energy F is analyzed in Appendix B. Assuming that $T_c^->T_c^+$ (i.e., $t_{3b}>0$), we find a second-order metal-SDW transition at temperature T_c^-, below which $u_{-\alpha}\neq 0$ and $u_{+\alpha}=0$. This transition opens a gap on the $-$ band, while the $+$ band remains gapless. This SDW phase is metallic. Note that the minimum of F corresponds to $|u_{j+}|=|u_{j-}|$. This implies that the SDW is linearly polarized (see Sec. III D).

If $4B_+B_--C^2\geqslant 0$, a second transition takes place at

$$T_c^{\mathrm{coex}}\simeq T_c^++\gamma(T_c^+-T_c^-), \tag{3.14}$$

where γ is a constant of order T^2/V^2. Below T_c^{coex}, both $u_{-\alpha}$ and $u_{+\alpha}$ are finite. $u_{+\alpha}$ opens a gap on the $+$ band, making the whole Fermi surface gapped, so that this low-temperature SDW is truly insulating. The transition is also of second order, since the order parameters $u_{-\alpha}$ and $u_{+\alpha}$ vary continuously at the transition.

Since $C/B_j=O(T^2/V^2)$, the condition $4B_+B_--C^2\geqslant 0$ is satisfied. Therefore, there is always coexistence of two SDW's at low temperature when the pairing is intraband. Eq. (3.14) shows that T_c^{coex} is well approximated by T_c^+.

SDW phases with wave vector $\mathbf{Q}_-,\mathbf{Q}_+$, or $\mathbf{Q}_-$ and $\mathbf{Q}_+$, have been previously obtained by Kishigi and coworkers.[10–12,18] However, the overall phase diagram (and in particular the existence of a SDW-metal-SDW transition) as a function of V has not been derived before.

D. Spin modulation $\langle\mathbf{S}(\mathbf{r})\rangle$

In this section, we determine the spin modulation $\langle\mathbf{S}(\mathbf{r})\rangle$ in the different SDW phases of the phase diagram. $\mathbf{S}(\mathbf{r})=(1/2)\Sigma_{\alpha,\sigma,\sigma'}\hat{\psi}^{\dagger}_{\alpha\sigma}(\mathbf{r})\boldsymbol{\tau}_{\sigma\sigma'}\hat{\psi}_{\alpha\sigma'}(\mathbf{r})$ is the spin-density operator and $\boldsymbol{\tau}=(\tau_x,\tau_y,\tau_z)$ stands for the Pauli matrices. Noting that $S_-=S_x-iS_y=\Sigma_{\alpha}\hat{\Delta}_{\alpha\uparrow}$, we obtain

$$\langle S_-(\mathbf{r})\rangle=\sum_{\alpha,j,p}\Delta_{\alpha}^{jp}\exp\left[i\alpha\left[\mathbf{Q}_j+(p-1)\frac{\mathbf{K}}{2}\right]\cdot\mathbf{r}\right]$$

$$=\sum_{\alpha,j}\Delta_{\alpha}^{j+}e^{i\alpha\mathbf{Q}_j\cdot\mathbf{r}}[1+(-1)^n\tan(\theta_j)], \tag{3.15}$$

where we have used $v_{j\alpha}=0$ to obtain the second line of Eq. (3.15). We consider the more general case where two SDW's can be present. We write Δ_{α}^{j+} as

$$\Delta_{\alpha}^{j+}=|\Delta_{\alpha}^{j+}|e^{i\varphi_{\alpha}^{j+}}, \tag{3.16}$$

and introduce the phases Θ_j and ϕ_j defined by

$$\varphi_{\alpha}^{j+}=\alpha\Theta_j-\phi_j. \tag{3.17}$$

According to the analysis of the free energy [Sec. III C and Appendix B], $|u_{j\alpha}|=|\Delta_{\alpha}^{j+}/\cos(\theta_j)|$ is independent of α. We, therefore, obtain

$$\langle S_-(\mathbf{r})\rangle = \sum_j 2|\Delta_+^{j+}|\cos(\mathbf{Q}_j\cdot\mathbf{r}+\Theta_j)e^{-i\phi_j} \times[1+(-1)^n\tan(\theta_j)]. \quad (3.18)$$

From Eq. (3.18), we deduce

$$\langle S_x(\mathbf{r})\rangle = \sum_j 2|\Delta_+^{j+}|\cos(\phi_j)\cos(\mathbf{Q}_j\cdot\mathbf{r}+\Theta_j) \times[1+(-1)^n\tan(\theta_j)],$$

$$\langle S_y(\mathbf{r})\rangle = \sum_j 2|\Delta_+^{j+}|\sin(\phi_j)\cos(\mathbf{Q}_j\cdot\mathbf{r}+\Theta_j) \times[1+(-1)^n\tan(\theta_j)]. \quad (3.19)$$

The phase ϕ_j determines the polarization of the SDW's, while Θ_j gives their positions with respect to the underlying crystal lattice. The free energy is independent of ϕ_j and Θ_j.

The ratio of the SDW amplitudes on even and odd chains is given by the factor $\delta_j=[1+\tan(\theta_j)]/[1-\tan(\theta_j)]$ shown in Fig. 8. δ remains close to one when V is weak ($V\leqslant V_{c1}$). $\delta\ll 1$ or $\delta\gg 1$ when V is strong [$\tan(\theta)\to\pm 1$ for $V\to\infty$] showing that the SDW's become mostly localized on even or odd chains (depending on the sign of θ). As expected, θ_+ and θ_- have opposite signs so that $\delta_+\simeq\delta_-^{-1}$.

Consider first the SDW phase occuring for a weak anion potential V (interband pairing). There is a single SDW with a wave vector $\mathbf{Q}=(2k_F,Q_y=\pi/b)$. The spin modulations on two neighboring chains are out of phase and the ratio δ of their amplitudes is close to one [Fig. 10(a)].

The SDW's corresponding to intraband pairing are also commensurate in the transverse direction, but with $(Q_y)_j=\pi/2b$; the spin modulations on two neighboring chains are in phase quadrature. Fig. 10(b) shows the spin modulation in the phase with a single SDW at wave vector $\mathbf{Q}_-$. The spin modulations below $T_c^{\rm coex}$ when two SDW's coexist is shown in Fig. 10c. The beating phenomenon is due to the fact that $(Q_x)_-\neq(Q_x)_+$.

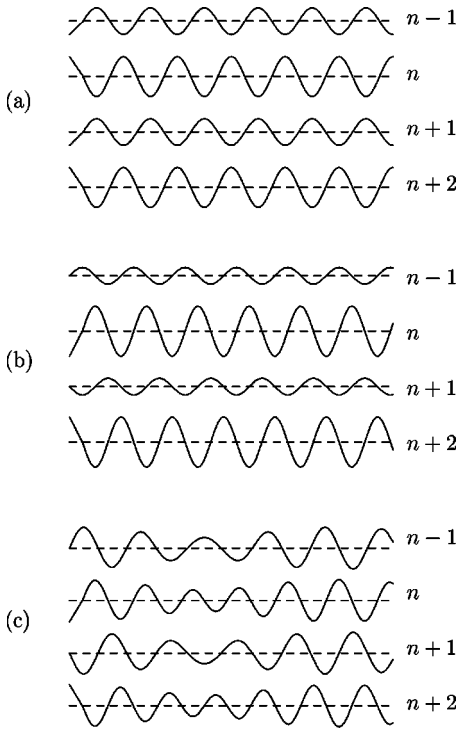

FIG. 10. Schematic representation of the spin modulation in the SDW phases (n denotes the chain index). (a) SDW phase for a weak anion potential V (interband pairing). (b) SDW phase for a strong anion potential (intraband pairing). (c) Low-temperature SDW phase ($T<T_c^{\rm coex}$) where two SDW's coexist.

IV. CONCLUSION

Anion ordering in the organic conductor $(TMTSF)_2ClO_4$ is expected to strongly influence the SDW instability. While a weak anion potential ($V\lesssim t_b$) suppresses the SDW instability, a strong anion potential leads to a rich phase diagram. When V becomes of the order of the interchain hopping amplitude ($V\sim t_b$), the effective hopping between even and odd chains is reduced. This opens up the possibility to have two successive instabilities when the temperature decreases. The first one primarily occurs on even (or odd) chains and destroys the Fermi surface of one of the two electronic bands. The other electronic band remains metallic in this phase. At lower temperature, a second transition occurs, primarily on odd (or even) chains, making the whole Fermi surface gapped.

According to Ref. 16, the gap due to the anion potential in the electronic dispersion is of the order of the transverse bandwidth, and the intraband nesting is almost perfect. In our model, this corresponds to a large value of V, i.e., $V\gtrsim t_b$. In this situation, one expects the ground state to be a SDW. Experimentally, the ground state is found to be a superconductor. There is no contradiction with our model though, since we did not consider the possibility of a superconducting transition. However, the observation of FISDW phases in $(TMTSF)_2ClO_4$ does require deviations from perfect nesting (otherwise, only the phase $N=0$ would be observed). This suggests that even when the anion potential is strong (large V in our model), important deviations form perfect nesting persist. The latter can be taken into account by considering t_{4b} in our model. Alternatively, the observation of the FISDW phases could indicate that the anion potential is weaker than what is predicted by quantum chemistry calculation. In our model, this would correspond to the region $V_{c1}<V<V_{c2}$, where the ground state is metallic. [Note that $V_{c1}=0$ if t_{2b} is large enough.]

Two successive transitions have been observed in $(TMTSF)_2ClO_4$ at high magnetic field.[6–8] The possibility that each of these transitions corresponds to an intraband pairing, thus partially destroying the Fermi surface, has been suggested early on.[6] Although our conclusions do not apply *stricto sensus* to the experimental situation, since they are restricted to the zero-field case, they indicate that this scenario could indeed take place in $(TMTSF)_2ClO_4$ at high field, in agreement with the conclusions of Refs. 10–12,18.

Beside the existence of two successive transitions at low temperature when V is strong enough, an important result obtained in this paper is the overall phase diagram as a func-

tion of V. In particular, we have obtained a SDW-metal-SDW transition at low temperature (Figs. 6 and 7).

Finally, we note that our results seriously call into question the validity of most of the previous works on the SDW transition at high magnetic field in $(TMTSF)_2ClO_4$. In the presence of anion ordering, the SDW order parameter necessarily has two Fourier components, and the standard Stoner criterion cannot be used anymore. Instead, one should consider the generalized Stoner criterion obtained in Sec. II B [Eq. (2.23)].

Note added. After completion of this work, we became aware of a related work by Zanchi and Bjeliš.[20] These authors have considered the effect of anion ordering on the SDW instability in $(TMTSF)_2ClO_4$ and obtained the transition temperature within RPA. Their results are similar to ours. However, they did not take into account a finite t_{3b} and did not study the coexistence of the two SDW's with wave vectors $\mathbf{Q}_+$ and $\mathbf{Q}_-$ at low temperature.

ACKNOWLEDGMENTS

We thank D. Zanchi for a useful comment on Ref. 20. One of the authors (KS) would like to thank Victor M. Yakovenko for support during the work.

APPENDIX A: QUARTIC CONTRIBUTION F_4 TO THE FREE ENERGY

Using Eqs. (2.6), (2.11), and (3.1), the quartic part of the free energy [Eq. (3.2)] can be written as in Eq. (3.10) with

$$\tilde{B}_\alpha(j_1,j_2,j_3,j_4;p_1,p_2,p_3,p_4)=\frac{g_2^4}{2N_\perp}\sum_{k_y}\sum_{j_5\cdots j_8}\sum_{p_5\cdots p_8}\sum_{p_5'\cdots p_8'}F_\alpha(j_1\cdots j_8,p_1\cdots p_8,p_5'\cdots p_8';k_y)$$
$$\times K_\alpha(j_1\cdots j_8;k_y)\sum_{n=-\infty}^{\infty}\delta_{\alpha(p_1-p_2+p_3+p_4)K/2+(-p_5-p_6-p_7-p_8+p_5'+p_6'+p_7'+p_8')K/2,n2\pi/b}, \tag{A1}$$

$$K_\alpha(j_1\cdots j_8;k_y)=\frac{T}{bL_x}\sum_{k_x,\omega}(i\omega-\epsilon_{\alpha,\mathbf{k}}^{j_5})^{-1}(i\omega-\epsilon_{\alpha,\mathbf{k}-\alpha\mathbf{Q}_{j_2}}^{j_6})^{-1}(i\omega-\epsilon_{\alpha,\mathbf{k}-\alpha\mathbf{Q}_{j_2}+\alpha\mathbf{Q}_{j_3}}^{j_7})^{-1}(i\omega-\epsilon_{\alpha,\mathbf{k}-\alpha\mathbf{Q}_{j_1}}^{j_8})^{-1}, \tag{A2}$$

$$F_\alpha(j_1\cdots j_8,p_1\cdots p_8,p_5'\cdots p_8';k_y)=\gamma_{k_y}^{j_5p_5}\gamma_{k_y}^{j_5p_5'}\gamma_{k_y-\alpha Q_{j_2y}-[\alpha(p_2-1)-p_5'+p_6]K/2}^{j_6p_6}$$
$$\times\gamma_{k_y-\alpha Q_{j_2y}-[\alpha(p_2-1)-p_5'+p_6]K/2}^{j_6p_6'}\gamma_{k_y-\alpha Q_{j_2y}+\alpha Q_{j_3y}-[\alpha(p_2+p_3)-p_5'+p_6-p_6'+p_7]K/2}^{j_7p_7}$$
$$\times\gamma_{k_y-\alpha Q_{j_2y}+\alpha Q_{j_3y}-[\alpha(p_2+p_3)-p_5'+p_6-p_6'+p_7]K/2}^{j_7p_7'}\gamma_{k_y-\alpha Q_{j_1y}-[\alpha(p_1-1)-p_5+p_8']K/2}^{j_8p_8}$$
$$\times\gamma_{k_y-\alpha Q_{j_1y}-[\alpha(p_1-1)-p_5+p_8']K/2}^{j_8p_8'}, \tag{A3}$$

where $N_\perp=L_y/b$ is the total number of chains. Since $v_{j\alpha}=0$, we have

$$\Delta_\alpha^{jp}=c_{jp}u_{j\alpha},$$

$$c_{j+}=\cos(\theta_j),\quad c_{j-}=\sin(\theta_j). \tag{A4}$$

Noting that the condition $\mathbf{Q}_{j_1}+\mathbf{Q}_{j_3}=\mathbf{Q}_{j_2}+\mathbf{Q}_{j_4}$ implies $j_1=j_2=j_3=j_4$ or $j_1=j_2=-j_3=-j_4$ or $j_1=-j_2=-j_3=j_4$, we obtain Eq. (3.11) with

$$B_j=\sum_{p_1\cdots p_4}c_{jp_1}c_{jp_2}c_{jp_3}c_{jp_4}\tilde{B}_\alpha(j,j,j,j;p_1,p_2,p_3,p_4),$$

$$C=\sum_j\sum_{p_1\cdots p_4}[c_{jp_1}c_{jp_2}c_{-jp_3}c_{-jp_4}$$
$$\times\tilde{B}_\alpha(j,j,-j,-j;p_1,p_2,p_3,p_4)+c_{jp_1}c_{-jp_2}c_{-jp_3}c_{jp_4}$$
$$\times\tilde{B}_\alpha(j,-j,-j,j;p_1,p_2,p_3,p_4)]. \tag{A5}$$

The main contribution to B_j comes from the type of diagrams shown in Fig. 9. This diagram involves the quantity,

$$K_\alpha(j_1=\cdots=j_8=i;k_y)=\frac{T}{bL_x}\sum_{k_x,\omega}(i\omega-\epsilon_{\alpha,\mathbf{k}}^{j})^{-2}$$
$$\times(i\omega-\epsilon_{\alpha,\mathbf{k}-\alpha\mathbf{Q}_j}^{j_-})^{-2}. \tag{A6}$$

To evaluate the order of magnitude of this diagram, we can assume perfect nesting. We then find

$$K_\alpha(j_1=\cdots=j_8=i;k_y)=\frac{T}{bL_x}\sum_{k_x,\omega}(\omega^2+\epsilon^j_{\alpha,\mathbf{k}}{}^2)^{-2}\sim\frac{1}{T^2}. \tag{A7}$$

A typical contribution to C is shown in Fig. 9. The order of magnitude of the diagram is given by

$$K_\alpha(j,j,-j,-j,j,j,j_7,j;k_y)$$
$$=\frac{T}{bL_x}\sum_{k_x,\omega}(i\omega-\epsilon^j_{\alpha,\mathbf{k}})^{-1}(i\omega-\epsilon^j_{\alpha,\mathbf{k}-\alpha\mathbf{Q}_j})^{-2}$$
$$\times(i\omega-\epsilon^{j_7}_{\alpha,\mathbf{k}-\alpha\mathbf{Q}_j+\alpha\mathbf{Q}_{-j}})^{-1}. \tag{A8}$$

To evaluate the preceding equation, we can assume perfect nesting in the j band,

$$K_\alpha(j,j,-j,-j,j,j,j_7,j;k_y)$$
$$=\frac{T}{bL_x}\sum_{k_x,\omega}(i\omega-\epsilon^j_{\alpha,\mathbf{k}})^{-1}(i\omega+\epsilon^j_{\alpha,\mathbf{k}})^{-2}$$
$$\times(i\omega-\epsilon^j_{\alpha,\mathbf{k}}+a)^{-1}\sim\frac{1}{V^2} \tag{A9}$$

where $|a|=|\epsilon^j_{\alpha,\mathbf{k}}-\epsilon^{j_7}_{\alpha,\mathbf{k}-\alpha\mathbf{Q}_j+\alpha\mathbf{Q}_{-j}}|\sim V$. We, therefore, conclude that $C/B_j=O(T^2/V^2)$.

APPENDIX B: MINIMUM OF THE FREE ENERGY F

The minimum of the free energy is obtained by solving the equations $\partial F/\partial u^*_{j\alpha}=0$,

$$u_{+\alpha}[A_+ +2B_+|u_{+\alpha}|^2+C|u_{-\alpha}|^2]=0,$$
$$u_{-\alpha}[A_- +2B_-|u_{-\alpha}|^2+C|u_{+\alpha}|^2]=0. \tag{B1}$$

In the metallic phase, $u_{j\alpha}=0$ and $F=0$. Below T_c^-, there is a phase with $u_{-\alpha}\neq 0$ and $u_{+\alpha}=0$. From Eqs. (B1) and (3.13), we deduce

$$|u_{-\alpha}|^2=-\frac{A_-}{2B_-},\quad F_-=-\frac{A_-^2}{2B_-}. \tag{B2}$$

Let us now consider a phase with two coexisting order parameters: $u_{+\alpha},u_{-\alpha}\neq 0$. Eqs. (B1) and (3.13) yield

$$|u_{+\alpha}|^2=\frac{-2A_+B_-+A_-C}{4B_+B_--C^2},$$

$$|u_{-\alpha}|^2=\frac{-2A_-B_++A_+C}{4B_+B_--C^2},$$

$$F_{\rm coex}=2\frac{-A_+^2B_--A_-^2B_++A_+A_-C}{4B_+B_--C^2}. \tag{B3}$$

This solution is allowed only if $|u_{j\alpha}|\geqslant 0$. The phase with two coexisting order parameters will be observed only if it has a lower free energy than the phase with a single order parameter, i.e., $F_{\rm coex}\leqslant F_-$:

$$2\frac{-A_+^2B_--A_-^2B_++A_+A_-C}{4B_+B_--C^2}\leqslant-\frac{A_-^2}{2B_-}. \tag{B4}$$

For $4B_+B_--C^2\leqslant 0$, this condition can be rewritten as $-(2A_-B_+-A_+C)^2\geqslant 0$, which shows that coexistence is not possible. For $4B_+B_--C^2\geqslant 0$, the condition $F_{\rm coex}\leqslant F_-$ becomes $-(2A_-B_+-A_+C)^2\leqslant 0$ and is, therefore, always satisfied. We thus conclude that coexistence occurs when the condition,

$$4B_+B_--C^2\geqslant 0, \tag{B5}$$

is fulfilled. The corresponding transition temperature $T_c^{\rm coex}$ is then determined from $|u_{j\alpha}|\geqslant 0$ [Eqs. (B3)]. When $C/B_j\ll 1$, $T_c^{\rm coex}$ is obtained from $|u_{+\alpha}|\geqslant 0$. Writing $A_j=a_j(T-T_c^j)$ and neglecting the temperature dependence of B_j and C, we obtain

$$T_c^{\rm coex}=T_c^+ +\frac{a_-C}{2a_+B_-}(T_c^{\rm coex}-T_c^-)$$
$$=T_c^+ +\gamma(T_c^+-T_c^-)+O(T^4/V^4), \tag{B6}$$

where $\gamma=a_-C/(2a_+B_-)$ is a constant of order $O(T^2/V^2)$.

[1] W. Kang, S.T. Hannahs, and P.M. Chaikin, Phys. Rev. Lett. **70**, 3091 (1993).

[2] For reviews, see P.M. Chaikin, J. Phys. I **6**, 1875 (1996); P. Lederer , *ibid.* **6**, 1899 (1996); V.M. Yakovenko and H.S. Goan, *ibid.* **6**, 1917 (1996).

[3] L.P. Gor'kov and A.G. Lebed', J. Phys. (France) Lett. **45**, L433 (1984); M. Héritier, G. Montambaux and P. Lederer, *ibid.* **45**, L943 (1984); K. Yamaji, J. Phys. Soc. Jpn. **54**, 1034 (1985); G. Montambaux, M. Héritier, and P. Lederer, Phys. Rev. Lett. **55**, 2078 (1985); A. Virosztek, L. Chen, and K. Maki, Phys. Rev. B **34**, 3371 (1986); G. Montambaux and D. Poilblanc, *ibid.* **37**, 1913 (1988).

[4] D. Poilblanc, G. Montambaux, M. Héritier, and P. Lederer, Phys. Rev. Lett. **58**, 270 (1987).

[5] V.M. Yakovenko, Phys. Rev. B **43**, 11 353 (1991).

[6] S.T. McKernan, S.T. Hannahs, U.M. Cheven, G.M. Danner, and P.M. Chaikin, Phys. Rev. Lett. **75**, 1630 (1995).

[7] J. Moser, Ph.D. thesis, Universit'è Paris-sud, 1999.

[8] O.-H. Chung, W. Kang, D.L. Kim, and C.H. Choi, Phys. Rev. B **61**, 11 649 (2000).

[9] A satisfying theoretical description of the phase diagram of $(TMTSF)_4ClO_4$ should show both the FISDW cascade at moderate field *and* the anomalous behavior above 18 T.
[10] K. Kishigi, K. Machida, and Y. Hasegawa, J. Phys. Soc. Jpn. **66**, 2969 (1997); K. Kishigi, *ibid.* **67**, 3825 (1998).
[11] Y. Hasegawa, K. Kishigi, and M. Miyazaki, J. Phys. Soc. Jpn. **67**, 964 (1998).
[12] M. Miyazaki, K. Kishigi, and Y. Hasegawa, J. Phys. Soc. Jpn. **68**, 313 (1999).
[13] A.G. Lebed' and P. Bak, Phys. Rev. B **40**, 11 433 (1989).
[14] T. Osada, S. Kagoshima, and N. Miura, Phys. Rev. Lett. **69**, 1117 (1992).
[15] L.P. Gor'kov and A.G. Lebed', Phys. Rev. B **51**, 3285 (1995).
[16] D. Le Péleven, J. Gaultier, Y. Barrans, D. Chasseau, F. Castet, and L. Ducasse, Eur. Phys. J. B **19**, 363 (2001).
[17] H. Yoshino, K. Saito, H. Nishikawa, K. Kikuchi, K. Kobayashi, and I. Ikemoto, J. Phys. Soc. Jpn. **66**, 2410 (1997).
[18] It should be pointed out that the work of Refs. 10–12 assumes a SDW order parameter with a single Fourier component, whereas there are (at least) two Fourier components in the presence of the anion potential (see text).
[19] g_1 does not play any role in the mean-field theory of SDW and we neglect Umklapp processes (g_3) in this work. For a detailed discussion of the possible role of Umklapp processes in the SDW phase of the Bechgaard salts, see N. Dupuis and V. Yakovenko, Phys. Rev. B **61**, 12 888 (2000).
[20] D. Zanchi and A. Bjeliš, cond-mat/0105530 (unpublished).